ADVANCED MATERIALS

Supporting Information

for *Adv. Mater.,* DOI: 10.1002/adma.202106436

Interface Engineering Between Multi-Elemental Alloy Nanoparticles and a Carbon Support Toward Stable Catalysts

*Tangyuan Li, Qi Dong, Zhennan Huang, Lianping Wu, Yonggang Yao, Jinlong Gao, Xizheng Wang, Haochuan Zhang, Dunwei Wang, Teng Li, Reza Shahbazian-Yassar, and Liangbing Hu**

Supporting Information for:

Interface Engineering between Multi-Elemental Alloy Nanoparticles and a Carbon Support toward Stable Catalysts

Tangyuan Li,[1] Qi Dong,[1] Zhennan Huang,[2] Lianping Wu,[3] Yonggang Yao,[1] Jinlong Gao,[1] Xizheng Wang,[1] Haochuan Zhang,[4] Dunwei Wang,[4] Teng Li,[3] Reza Shahbazian-Yassar,[2] Liangbing Hu[1,*]

1. Department of Materials Science and Engineering, University of Maryland, College Park, Maryland 20742, USA
2. Department of Mechanical and Industrial Engineering, University of Illinois at Chicago, Chicago, Illinois 60607, USA
3. Department of Mechanical Engineering, University of Maryland, College Park, Maryland 20742, USA
4. Department of Chemistry, Boston College, Chestnut Hill, Massachusetts 02467, USA

This supporting information contains:

- Supplementary Figures S1–S19
- Supplementary Tables S1

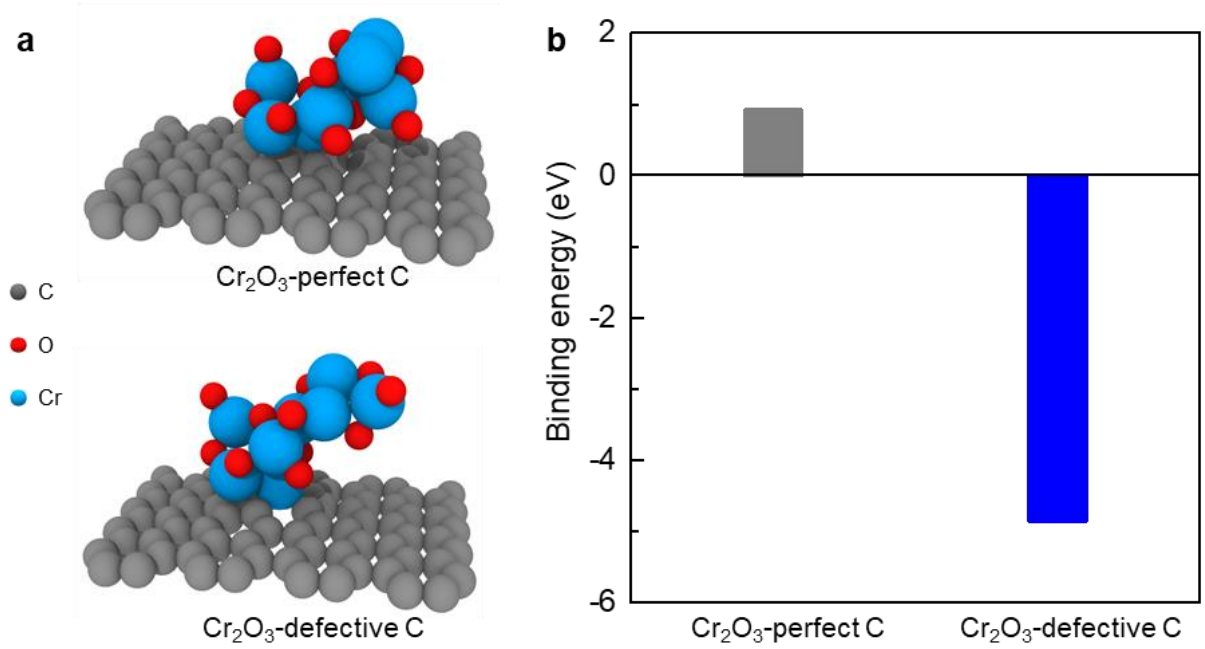

Figure S1. (a) The atomic structure and (b) binding energy of Cr_2O_3 on the perfect graphene and defective graphene, respectively. The binding energy of the Cr_2O_3 on perfect graphene is positive, indicating the Cr_2O_3-perfect graphene is an unstable system, while Cr_2O_3 prefers to form on the defective graphene due to the negative binding energy. The defective carbon with/without Cr_2O_3 as the support is used to calculate the binding energies of PdRuRh on the two substrates.

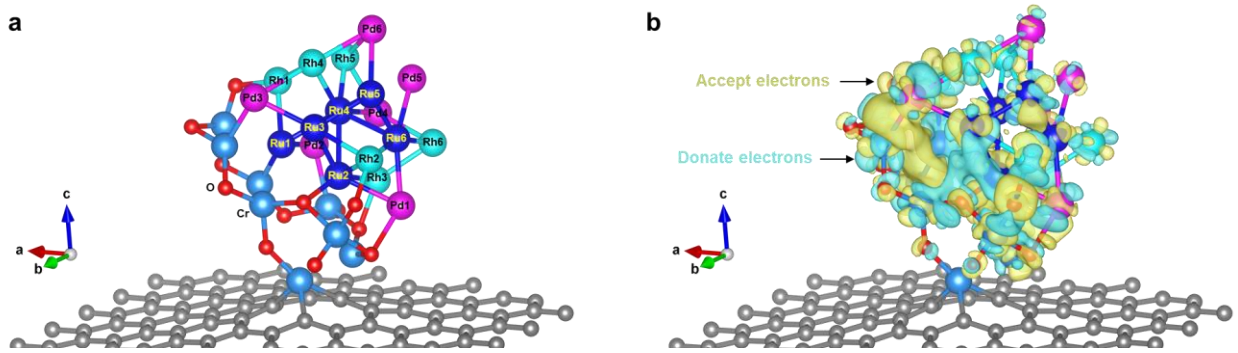

Figure S2. (a) Atomic structure and (b) charge density difference of the MEA-Cr_2O_3-carbon system. The MEA PdRuRh nanoparticle contains 6 Pd atoms, 6 Ru atoms, and 6 Rh atoms. The yellow area (Figure S2b) means accepting electrons, while the green area represents donating electrons. For the charge distribution between Cr and the metal atoms, both metal atoms and Cr are losing electrons, leading to a negative charge density difference; meanwhile, the area between Cr and the metal atoms accepts electrons, leading to a positive charge density difference. This means that the Cr and metal atoms are sharing electrons, and they have directional bond. Hence, the bond between the metal atoms and Cr is considered as metallic and covalent bond. For the charge distribution between O and metal atoms, metal atoms tend to donate electrons, and O atoms tend to accept electrons, which results in the formation of ionic bond between the metal and O atoms.

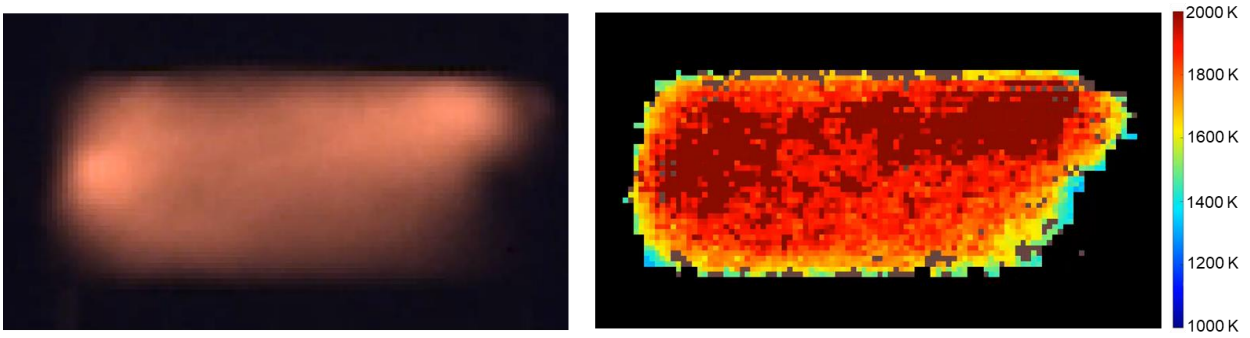

Figure S3. An optical image and its corresponding spatial temperature distribution of the precursor-loaded carbon nanofiber film during temperature measurement. The film can be heated up to 1800 K within 0.05 s.

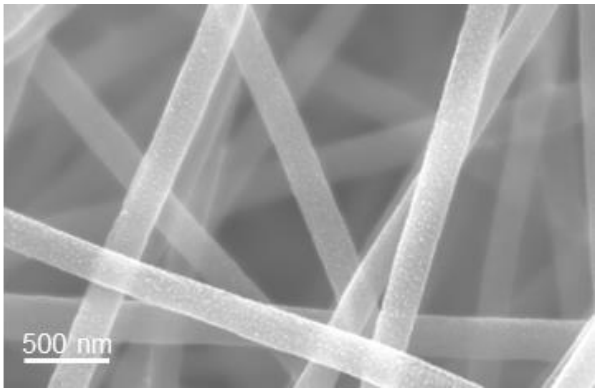

Figure S4. SEM image for PtPdIrRuRh-TiO_2-carbon nanofiber, synthesized by the temperature profile of ~1800 K and ~0.01 s. The average sizes of MEA and oxide nanoparticles for the sample synthesized by ~1800 K and ~0.01 s are lower than that of the one synthesized by ~1800 K and ~0.05 s (Figure 2c). We can tune the nanoparticle size by tuning the heating time: a shorter duration results in smaller nanoparticles.

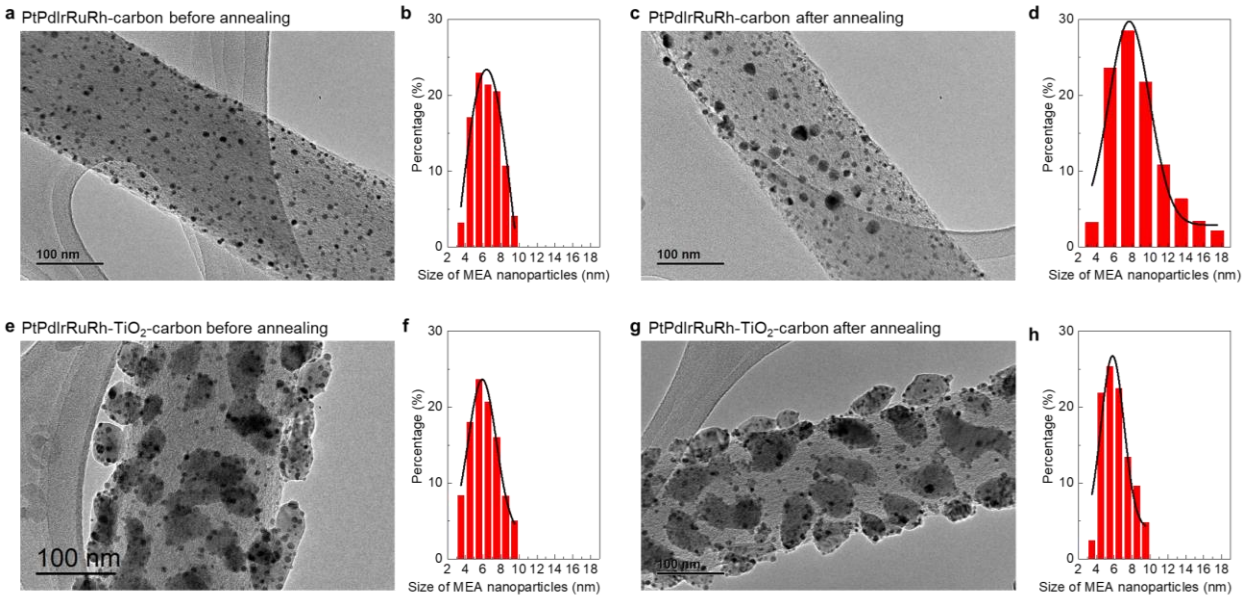

Figure S5. (a, c) TEM images and (b, d) size distribution of PtPdIrRuRh-carbon nanofiber (a, b) before and (c, d) after *ex situ* thermal annealing at 1023 K for 30 min under argon atmosphere using a furnace. (e, g) TEM images and (f, h) size distribution of PtPdIrRuRh-TiO_2-carbon nanofiber (e, f) before and (g, h) after *ex situ* thermal annealing at 1023 K for 30 min under argon atmosphere using the furnace. The introduction of oxide into the MEA-carbon system has no obvious effect on the morphology and size of MEA nanoparticles. In addition, the PtPdIrRuRh nanoparticles dispersed on carbon show particle agglomeration after *ex situ* heating, which indicates the weak binding between PtPdIrRuRh and carbon. However, the PtPdIrRuRh-TiO_2-carbon nanofiber sample still maintains uniform dispersion after high-temperature annealing, and the oxide-supported multimetallic nanoparticles show superior stability.

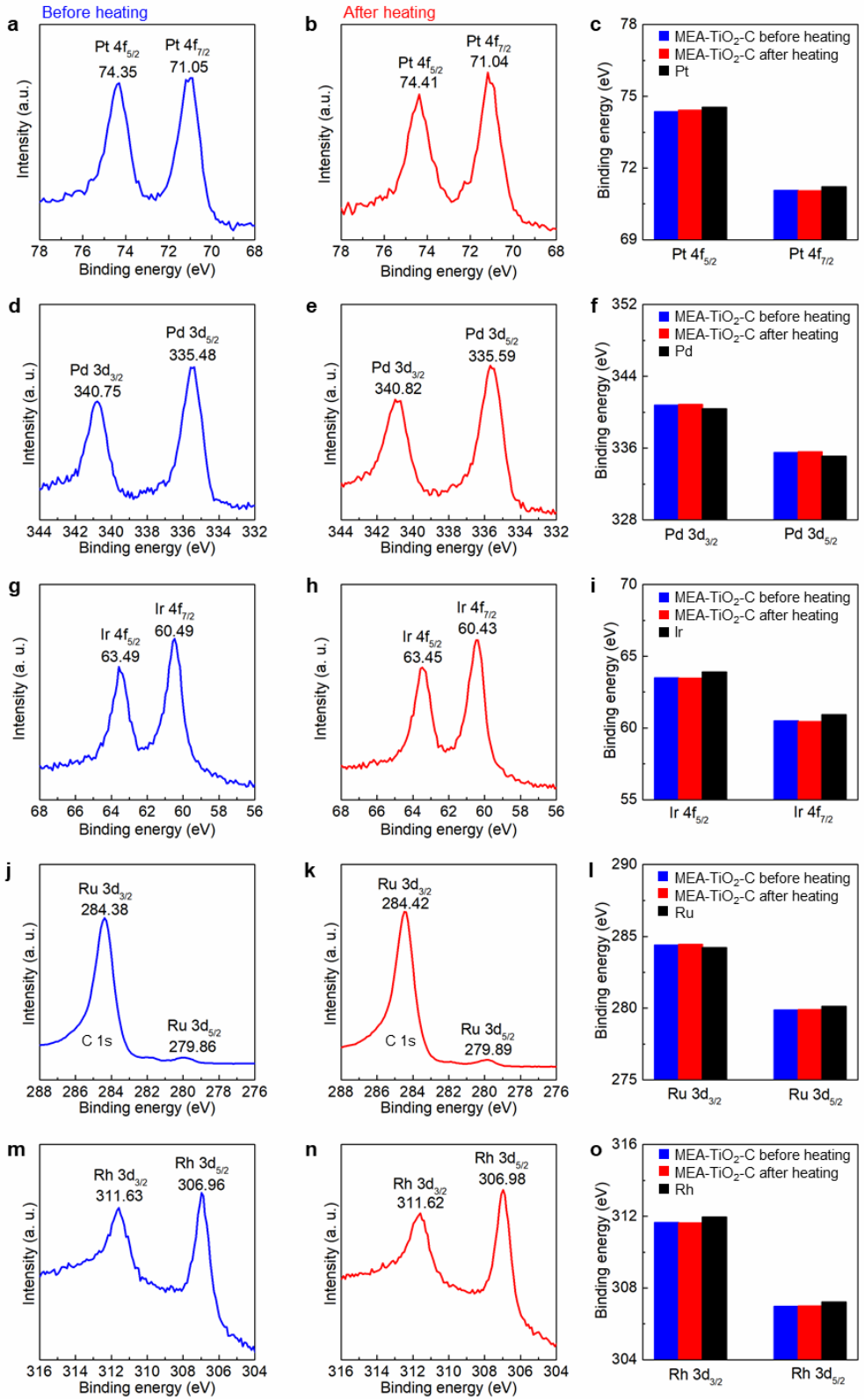

Figure S6. Pt 4f, Pd 3d, Ir 4f, Ru 3d, and Rh 3d XPS spectra of PtPdIrRuRh-TiO_2-C samples before and after *ex situ* heating at 1023 K, and comparison of Pt 4f, Pd 3d, Ir 4f, Ru 3d, and Rh 3d

XPS peaks for unary metal (*J. F. Moulder, et al., Handbook of X-ray Photoelectron Spectroscopy, 1992*) Pt, Pd, Ir, Ru, Rh, and our sample before and after heating. There are almost no changes on the binding energies of Pt $4f_{7/2}$, Pt $4f_{5/2}$, Pd $3d_{5/2}$, Pd $3d_{3/2}$, Ir $4f_{7/2}$, Ir $4f_{5/2}$, Ru $3d_{5/2}$, Ru $3d_{3/2}$, Rh $3d_{5/2}$, and Rh $3d_{3/2}$ for the PtPdIrRuRh-TiO_2-C sample before and after heating. The XPS results confirm that Pt, Pd, Ir, Ru, and Rh are all in the metallic state.

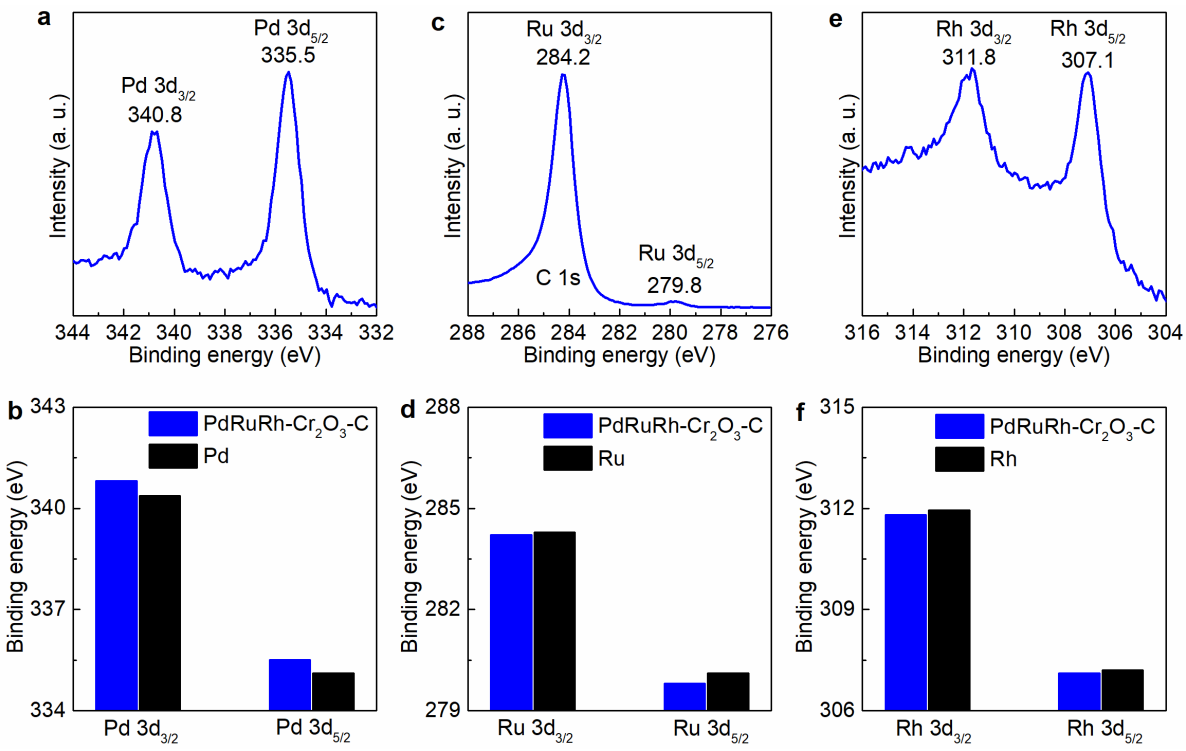

Figure S7. Pd 3d, Ru 3d, and Rh 3d X-ray photoelectron spectroscopy (XPS) spectra of the PdRuRh-Cr_2O_3-C catalyst, and comparison of Pd 3d, Ru 3d, and Rh 3d XPS spectra of unary metal (*J. F. Moulder, et al., Handbook of X-ray Photoelectron Spectroscopy, 1992*) Pd, Ru, Rh, and PdRuRh-Cr_2O_3-C samples. The binding energies of Pd $3d_{5/2}$, Pd $3d_{3/2}$, Ru $3d_{5/2}$, Ru $3d_{3/2}$, Rh $3d_{5/2}$, and Rh $3d_{3/2}$ electrons are recorded at 335.5 eV, 340.8 eV, 279.8 eV, 284.2 eV, 307.1 eV, and 311.8 eV in our PdRuRh-Cr_2O_3-C sample, respectively, confirming the existence of Pd, Ru, and Rh in the metallic state. Compared with unary metal Pd, Ru, and Rh, Pd 3d XPS peaks move toward higher binding energies, while both Ru 3d and Rh 3d XPS peaks slightly shift to lower binding energies. The results suggest that Pd donates electrons while Ru and Rh accept electrons in MEA nanoparticles. In other words, Pd is relatively electron-deficient while Ru and Rh are relatively electron-rich.

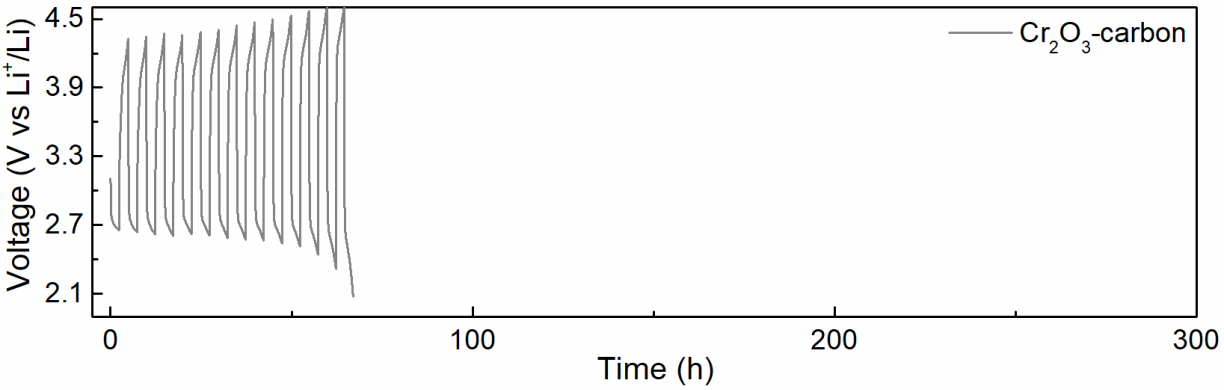

Figure S8. Cycling performance of the Li-O_2 cell using the Cr_2O_3-carbon cathode. The cell using Cr_2O_3-carbon shows high overpotential, and only lasted for 12 cycles.

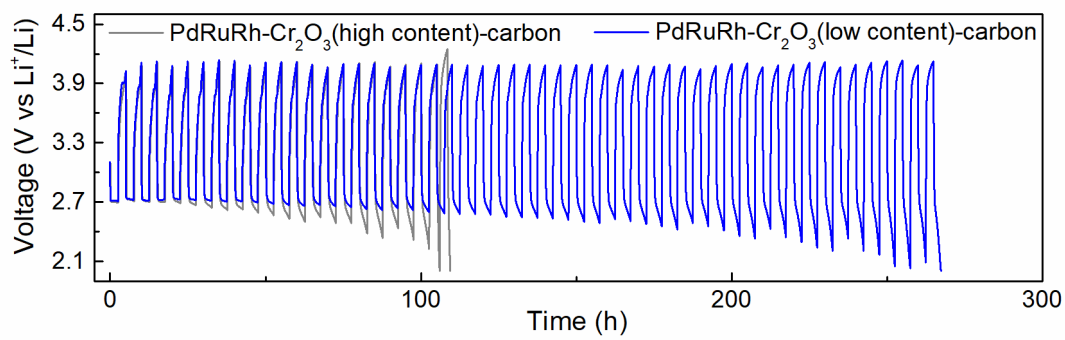

Figure S9. Cycling performances of the Li-O_2 cell using the PdRuRh-Cr_2O_3-carbon cathodes with different loading contents of Cr_2O_3 (i.e., ~10wt% and ~20wt%).

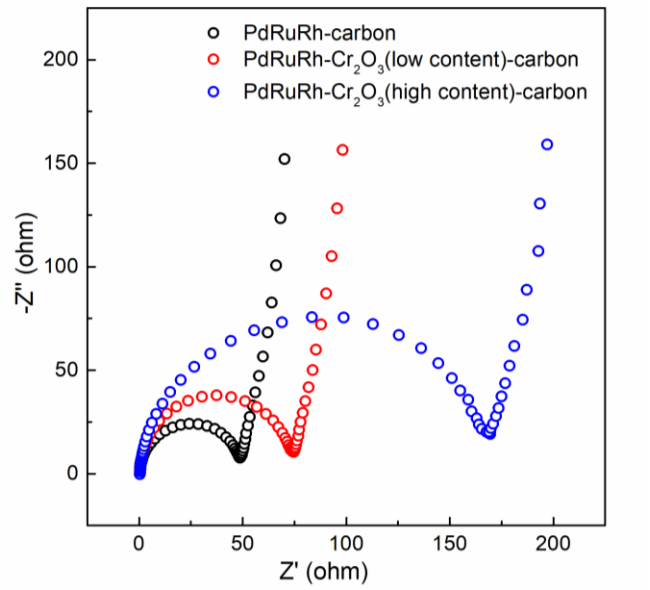

Figure S10. Typical impedance plots of PdRuRh-carbon, PdRuRh-Cr_2O_3(low content of ~10wt%)-carbon, and PdRuRh-Cr_2O_3(high content of ~20wt%)-carbon. PdRuRh-carbon and PdRuRh-Cr_2O_3(low content of ~10wt%)-carbon show lower charge-transfer resistance values of 50.1 Ω and 72.3 Ω, respectively, suggesting fast charge transfer behavior. This is beneficial for the improvement of ORR and OER catalytic performance in Li-O_2 batteries. In contrast, the PdRuRh-Cr_2O_3(high content of ~20wt%)-carbon with more oxides exhibits a higher charge-transfer resistance of 170.5 Ω, leading to poor catalytic performance.

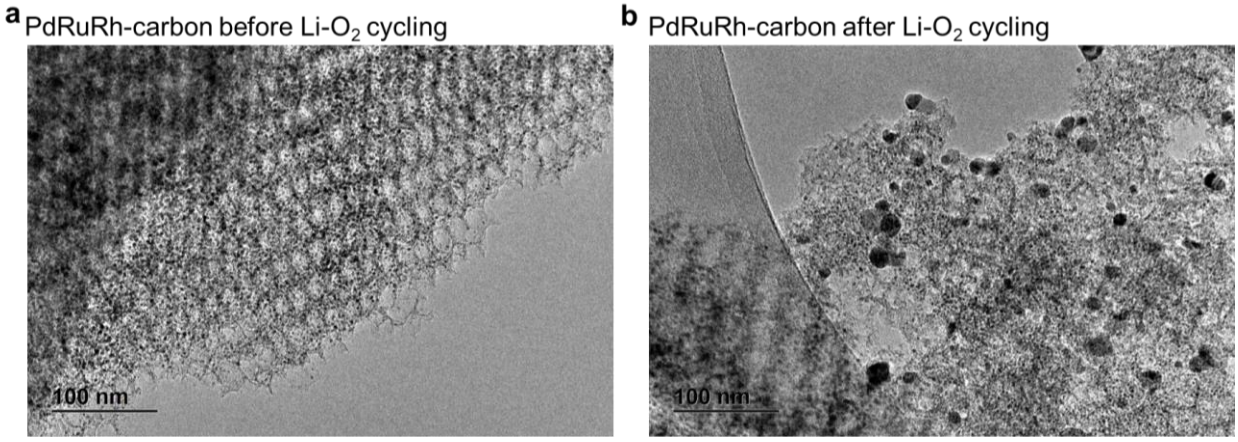

Figure S11. TEM images of 3DOm carbon-supported PdRuRh nanoparticles (a) before and (b) after Li-O_2 cycling test. The sample after cycling shows obvious particle agglomeration, causing a substantial loss in the activity.

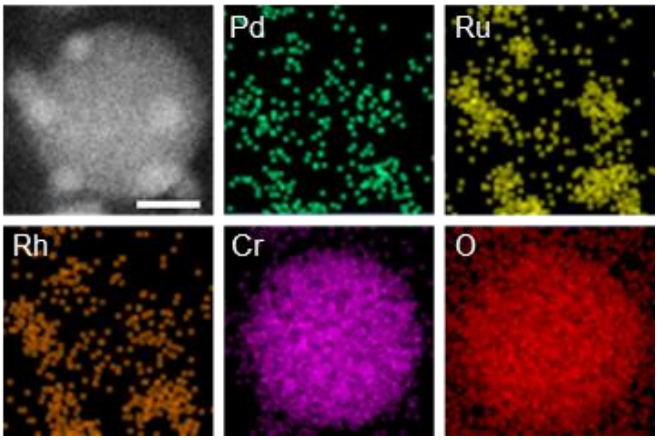

Figure S12. Elemental mappings of PdRuRh-Cr_2O_3-carbon before Li-O_2 cycling, indicating the uniform dispersion and homogenous mixing of the MEA PdRuRh nanoparticles. Scale bar: 10 nm.

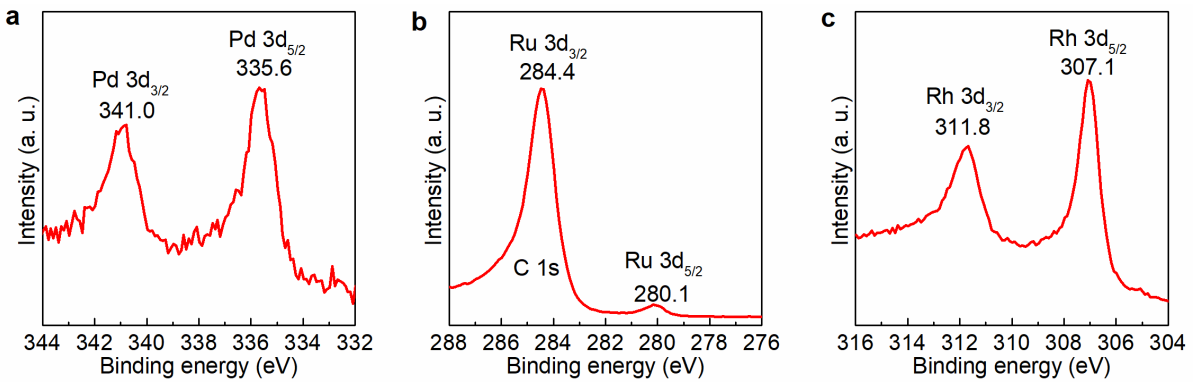

Figure S13. Pd 3d, Ru 3d, and Rh 3d XPS spectra of the PdRuRh-Cr_2O_3-C catalyst after Li-O_2 cycling. The binding energies of Pd $3d_{5/2}$, Pd $3d_{3/2}$, Ru $3d_{5/2}$, Ru $3d_{3/2}$, Rh $3d_{5/2}$, and Rh $3d_{3/2}$ electrons are recorded at 335.6 eV, 341.0 eV, 280.1 eV, 284.4 eV, 307.1 eV, and 311.8 eV, respectively, confirming the existence of Pd, Ru, and Rh in the metallic state.

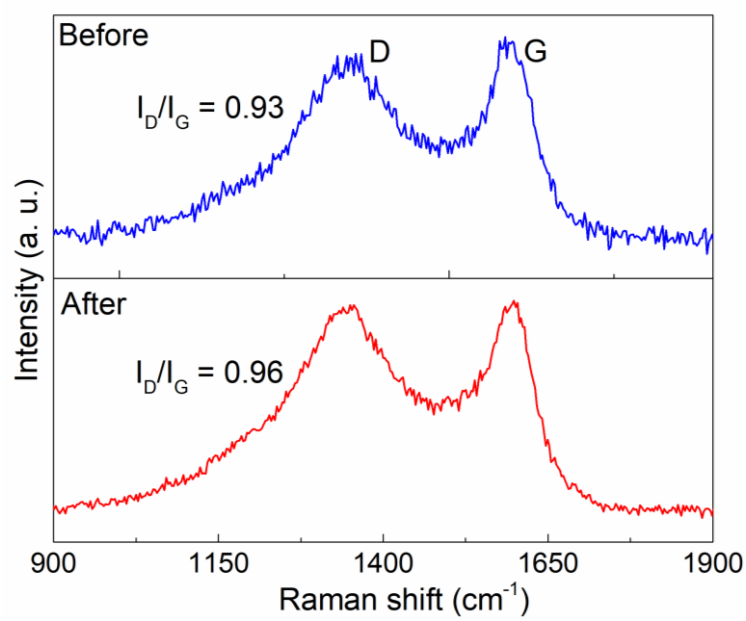

Figure S14. Raman spectra of the PdRuRh-Cr_2O_3-carbon samples before and after the Li-O_2 battery cycling tests. The I_D/I_G ratios of the sample before and after cycling are 0.93 and 0.96, respectively, indicating minimal change of the carbon substrate.

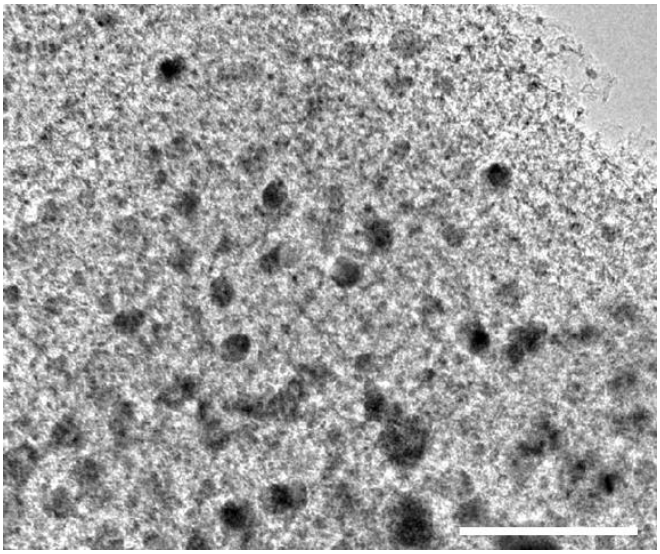

Figure S15. TEM image of PdRuRh-Cr_2O_3-carbon after *ex situ* thermal annealing at 1023 K for 30 min under argon atmosphere using a furnace. The heterostructure PdRuRh-Cr_2O_3 nanoparticles still maintain uniform dispersion on carbon after annealing. Scale bar: 100 nm.

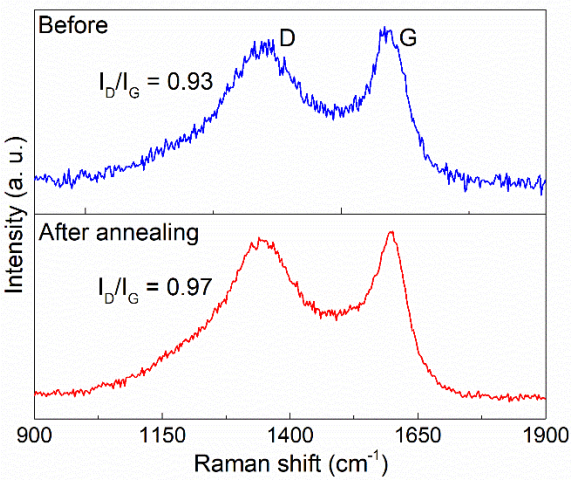

Figure S16. Raman results of the PdRuRh-Cr_2O_3-carbon samples before and after before and after *ex situ* heating at 1023 K for 30 min under argon atmosphere using a furnace. The I_D/I_G ratios of the sample before and after cycling are 0.93 and 0.97, respectively, indicating the minimal change of the carbon substrate.

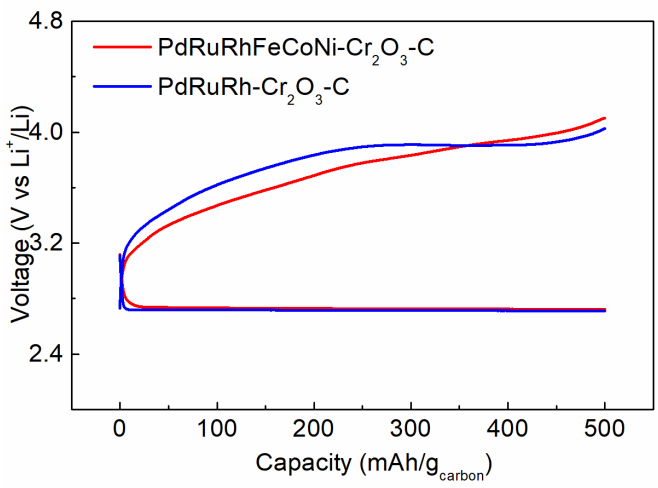

Figure S17. The discharge and recharge profiles during the 1st cycle of Li-O_2 battery test cells using PdRuRh-Cr_2O_3-C and PdRuRhFeCoNi-Cr_2O_3-C. Their profiles demonstrate comparable overpotentials, therefore similar catalytic activity by the MEA catalysts.

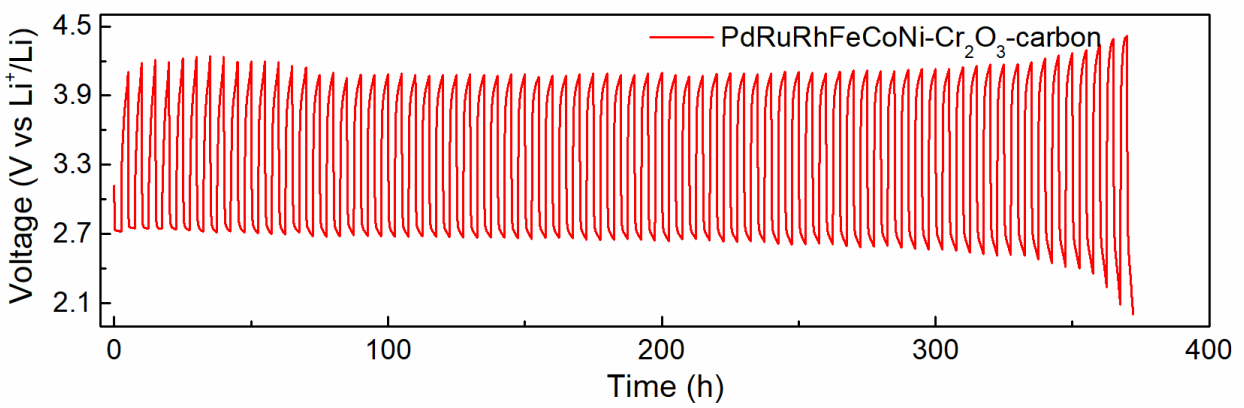

Figure S18. Cycling performance of the Li-O_2 cell using the PdRuRhFeCoNi-Cr_2O_3-carbon catalytic cathode. The cell lasted for 74 cycles (~370 hours).

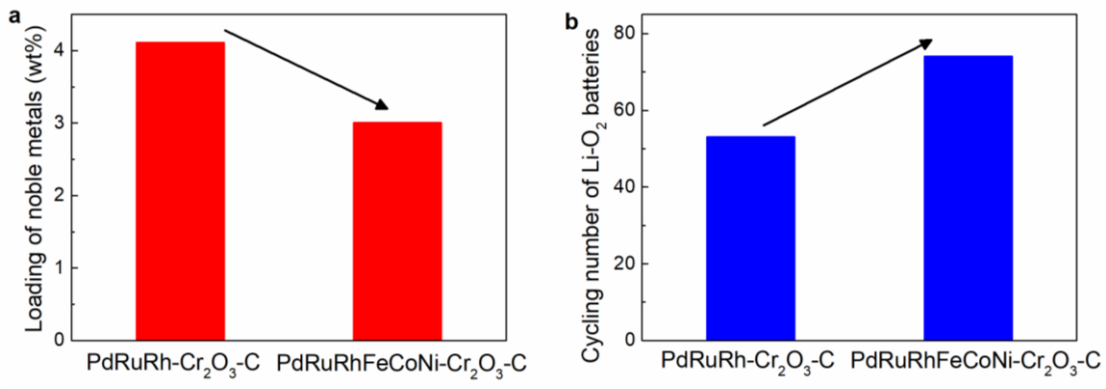

Figure S19. (a) Loading contents (tested by ICP-MS) of used noble metals (b) and cycling number of Li-O_2 batteries for the PdRuRh-Cr_2O_3-carbon and PdRuRhFeCoNi-Cr_2O_3-carbon samples. We have shown the low contents (3.00 wt%) of used noble elements in PdRuRhFeCoNi-Cr_2O_3-carbon compared with PdRuRh-Cr_2O_3-carbon (4.11 wt%), resulting from the introduction of non-noble Fe, Co, and Ni. The PdRuRhFeCoNi-Cr_2O_3-carbon sample also demonstrates excellent cycling stability of Li-O_2 batteries, where the noble elements ensure the catalytic activity while the non-noble metals improve the catalytic stability due to enhanced mixing entropy.

Table S1. Bader charge transfer of Pd, Ru, and Rh in the PdRuRh-Cr_2O_3-C system. Among these atoms, Pd1, Pd2, Pd3, Ru1, Ru2, Rh1, Rh2, and Rh3 atoms directly interact with Cr_2O_3 (see Figure S2). Higher charge transfer of Ru indicates that Ru element is more preferable among multiple elements to interact with the oxide.

Atom	Pd1	Pd2	Pd3	Pd4	Pd5	Pd6
Charge transfer	-0.02	0.15	0.25	0.10	0.09	0.16
Atom	Ru1	Ru2	Ru3	Ru4	Ru5	Ru6
Charge transfer	0.25	-0.30	-0.20	-0.32	-0.14	-0.21
Atom	Rh1	Rh2	Rh3	Rh4	Rh5	Rh6
Charge transfer	-0.13	-0.15	-0.19	0.04	0.02	0.06